SPIN
Vol. 2, No. 3 (2012) 1240003 (12 pages)

DOI: 10.1142/S2010324712400036

RECENT PROGRESS OF PERPENDICULAR ANISOTROPY MAGNETIC TUNNEL JUNCTIONS FOR NONVOLATILE VLSI

SHOJI IKEDA[*,†,¶], HIDEO SATO[*], MICHIHIKO YAMANOUCHI[*,†], HUADONG GAN[*], KATSUYA MIURA[*,†,§], KOTARO MIZUNUMA[†], SHUN KANAI[†], SHUNSUKE FUKAMI[*], FUMIHIRO MATSUKURA[*,†,‡], NAOKI KASAI[*] and HIDEO OHNO[*,†,‡]

[*]*Center for Spintronics Integrated Systems, Tohoku University*
2-1-1 Katahira, Aoba-ku, Sendai 980-8577, Japan

[†]*Laboratory for Nanoelectronics and Spintronics*
Research Institute of Electrical Communication
Tohoku University, 2-1-1 Katahira, Aoba-ku, Sendai 980-8577, Japan

[‡]*WPI Advanced Institute for Materials Research, Tohoku University*
Katahira 2-1-1, Aoba-ku, Sendai 980-8577, Japan

[§]*Central Research Laboratory, Hitachi, Ltd.*
Kokubunji, Tokyo 185-8601, Japan
[¶]*sikeda@riec.tohoku.ac.jp*

Received 23 August 2012
Accepted 13 September 2012
Published 4 December 2012

We review recent developments in magnetic tunnel junctions with perpendicular easy axis (p-MTJs) for nonvolatile very large scale integrated circuits (VLSIs). So far, a number of material systems such as rare-earth/transition metal alloys, $L1_0$-ordered (Co, Fe)−Pt alloys, Co/(Pd, Pt) multilayers, and ferromagnetic-alloy/oxide stacks have been proposed as electrodes in p-MTJs. Among them, p-MTJs with single or double ferromagnetic-alloy/oxide stacks, particularly CoFeB−MgO, were shown to have high potential to satisfy major requirements for integration.

Keywords: Magnetic tunnel junction; perpendicular anisotropy; spin transfer torque; CoFeB; MgO.

1. Introduction

Increase of static power dissipation is becoming a serious obstacle in enhancing the performance of very large scale integrated circuits (VLSIs) due to increase of leakage current with scaling complementary metal oxide semiconductor (CMOS) technology to advanced nodes. In addition, increase in the length of global interconnection in VLSIs leads to further increase of both power consumption and interconnection delay. Nonvolatile memory fabricated in back-end-of-line process of VLSI potentially offers the reductions of both power and delay. The nonvolatile memory to be used with

VLSI is required to satisfy a capability of shorter access time than 10 ns, virtually unlimited endurance and scalable writing scheme at a small dimension comparable to the employed CMOS technology, in addition to nonvolatility. Nonvolatile memory using magnetic tunnel junctions (MTJs) with spin transfer torque (STT) switching[1,2] is currently the only candidate in emerging nonvolatile memory technology that could satisfy all the requirements mentioned above. Thus, magnetoresistive random-access memories (MRAMs)[3–9] and logic circuits[2,10–16] embedding MTJs are being developed actively. In this review, we focus on results of MTJs, especially those with perpendicular easy axis (p-MTJs), for nonvolatile VLSIs such as MRAM and spintronics-based logic chips, and discuss future prospects of spintronics materials for p-MTJ.

2. Magnetic Tunnel Junction

Figure 1(a) shows a schematic diagram of typical one MTJ-one transistor cell as a memory cell architecture in MRAM with STT writing (STT-MRAM). In the MTJ, information is stored as the magnetization direction in one of the two ferromagnetic layers separated by a thin tunnel barrier, which is called as recording layer. The other layer, called as reference layer, is designed in such a way

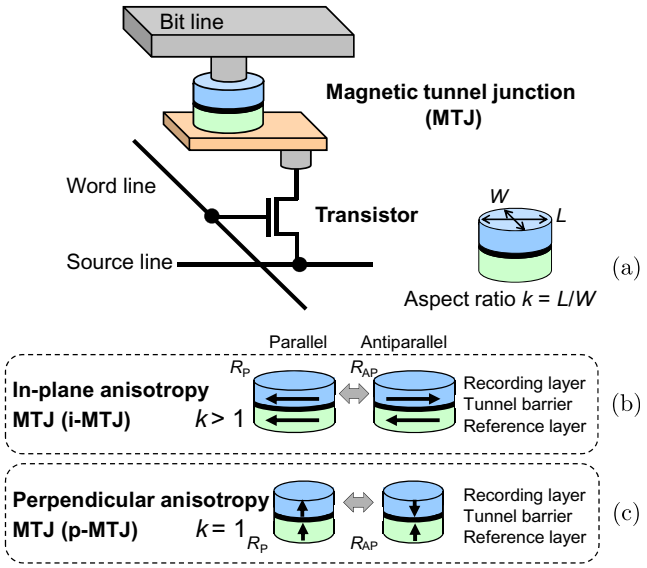

Fig. 1. Schematic diagram of (a) one MTJ-one transistor cell, magnetization configuration of (b) MTJ with in-plane easy axis (i-MTJ) with aspect ratio $k = L/W > 1$, and (c) that with perpendicular easy axis (p-MTJ) with $k = 1$.

that it is hard to reverse its magnetization. There are two types of MTJ in relation to the direction of magnetic easy axes of the two magnetic electrodes. One is MTJ with in-plane easy axis [i-MTJ, see Fig. 1(b)] and the other is that with perpendicular easy axis [p-MTJ, see Fig. 1(c)].

Read and write operations are performed by applying current into the MTJ which is selected by the bit line and word line connected to a transistor, as shown in Fig. 1(a). STT writing is based on transfer of spin angular momentum from conduction electrons to the magnetization of magnetic layer.[17–20] Antiparallel (AP) and parallel (P) magnetization configurations between the recording and reference layers can be controlled by the direction of current passing through the MTJ. Resistance of these MTJs commonly varies depending on the relative magnetization directions of the recording and reference layers due to spin-dependent tunneling involved in the transport between the majority and minority spin states. This resistance change ratio is called as tunnel magnetoresistance (TMR) ratio, and defined as TMR ratio $= \Delta R/R = (R_{AP} - R_P)/R_P$, where R_{AP} and R_P are the resistance for AP and P magnetization configurations [see Figs. 1(b) and 1(c)], respectively. High TMR ratios up to 604% at room temperature (RT) and 1144% at 5 K, approaching the theoretically predicted value,[21,22] have been observed in MgO barrier MTJs.[23–28]

A high performance MTJ needs to satisfy five requirements at least: (1) small size (F nm, F: feature size), (2) low current for STT switching (intrinsic critical switching current $I_{C0} < F\mu$A), (3) high TMR ratio (>100%), (4) high thermal stability factor of the recording layer $\Delta = E/k_BT$ (>40, where E denotes energy barrier between P and AP configurations, k_B is the Boltzmann constant and T is the absolute temperature) and finally (5) capability to withstand annealing treatment at the temperature (T_a) of 350°C at least required for standard semiconductor processing without losing its high TMR ratio.

Figure 2 shows the MRAM development trend. The STT-MRAMs with i-MTJs have reached capacity up to 64 Mb.[6,9,29,30] In principle, STT-MRAMs with p-MTJs can achieve lower I_{C0} and higher Δ than STT-MRAMs with i-MTJs, because demagnetizing field reduces the I_{C0} while Δ can be made high using high magnetic anisotropy materials. Because of this, STT-MRAMs with

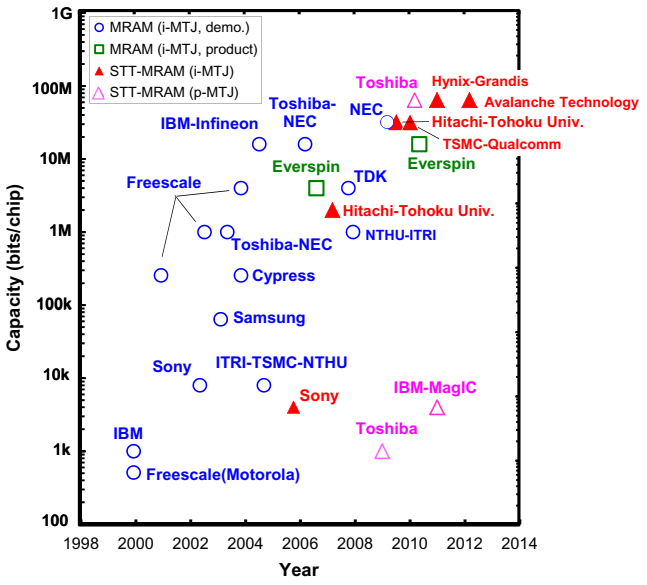

Fig. 2. MRAM development trend. Here, MRAM stands for those that employ the magnetic-field writing, while STT-MRAM stands for those that employ the spin transfer torque writing.

p-MTJs in recent years have been pursued and demonstrated, as shown in Fig. 2.[5,7,8] The I_{C0} for p-MTJ with coherent magnetization reversal can be expressed as follows;

$$I_{C0} = \alpha\gamma e M_S H_K^{eff} V/\mu_B g = 2\alpha\gamma e E/\mu_B g, \quad (1)$$

where α is the magnetic damping constant, γ the gyromagnetic ratio, e the elementary charge, M_S the saturation magnetization, H_K^{eff} the effective anisotropy field including demagnetizing field, V the volume of recording layer, μ_B the Bohr magnetron and g a function of the spin polarization of the tunnel current and the relative magnetization angle between the recording and the reference layers.[17,18,31–33] For the magnetic electrode materials in p-MTJ with reduced dimensions, low α is needed in order to realize low switching current ($I_{C0} = F\mu$A) while maintaining high E, i.e., high Δ.

3. Ferromagnetic Electrodes for p-MTJs

To attain perpendicular anisotropy, a number of material systems have been explored as electrodes, including rare-earth/transition metal alloys, $L1_0$-ordered (Co, Fe)−Pt alloys, multilayers and so on. We review the developments of these electrodes.

3.1. *Rare-earth/transition metal alloys*

In 2002, Nishimura *et al.* reported the TMR ratio of 55% at RT in GdFeCo/CoFe/Al_2O_3/CoFe/TbFeCo p-MTJ, which is the first demonstration of p-MTJ.[34] TMR ratio of 74% reported in double AlO_x barrier p-MTJ with GdFeCo/AlO_x/GdFeCo/FeCo/AlO_x/FeCo/TbFeCo stack structure.[35] Subsequent experiments demonstrated TMR ratio of 64% in GdFeCo/Fe/MgO/Fe/TbFeCo p-MTJ,[36] and of 70% in Pr_6O_{11} barrier p-MTJ with different TbCoFe composition electrodes.[37] Nakayama *et al.* observed STT switching with 4.7 MA/cm^2 in 130 nm-diameter TbFeCo/CoFeB/MgO/CoFeB/TbFeCo p-MTJ with Δ of 107, although TMR ratio showed a low value of 15%,[38] mainly due to the lack of appropriate annealing. Rare-earth-based alloys have the following advantages; the alloys with amorphous phase can obtain easily a perpendicular magnetic easy axis independent of underlayer material, and have low magnetization.[39,40] On the other hand, the lack of processing stability (for annealing, etching and passivation processes) and the high α need to be addressed to be a candidate for electrode material of high performance p-MTJ.[32,41]

3.2. *$L1_0$-ordered (Co, Fe)−Pt alloys*

$L1_0$-order (Co, Fe)−Pt alloys is one of candidates for p-MTJ with small dimension because of its large magnetic anisotropy energy density of more than 10^6 J/m^3.[42,43] In 2006, Seki *et al.* reported STT switching with current density of the order of 10^8A/cm^2 in current perpendicular to plane giant magnetoresistance (CPP-GMR) pillars with $L1_0$-FePt electrodes exhibiting perpendicular anisotropy of the order of 10^6 J/m^3 around the same time as demonstrations of MTJs with multilayer electrodes as mentioned in next section.[44] MgO barrier p-MTJ with $L1_0$-CoPt electrodes showed TMR ratio of 6% at RT (13% at 10 K).[45] These results required an MgO (001) single crystal substrate and a high annealing temperature (T_a) of 500−600°C. Yoshikawa *et al.* succeeded in obtaining high TMR ratios at RT of 120% at $T_a = 500$°C (58% at $T_a = 400$°C) in $L1_0$-FePt/MgO p-MTJs sputtered on thermally oxidized Si wafer.[46] Based on first principles calculations, the TMR ratio evaluated for the junction with the Fe-terminated interface exceeds 380%.[47] Thus, it was shown from both experimental and theoretical studies that FePt is a candidate of

materials for high TMR ratio. It was, however, necessary to reduce the optimal heat treatment temperature for realizing high TMR ratio over 100% to 350°C−400°C for VLSI applications. A higher TMR ratio of 202% at RT was reported in composite p-MTJ structure with $L1_0$-FePt/CoFeB/MgO/CoFeB/Co-based superlattice.[48] Kishi *et al.* demonstrated STT switching with 49 μA and Δ of 56 in the MgO barrier p-MTJ with the recording layer size of 50−55 nm in diameter using $L1_0$ ordered alloy with $\alpha = 0.028$.[5] Subsequently, it was reported that 50 nm ϕ p-MTJs with Fe alloy with doping of Pt and/or other elements obtained switching current around 10 μA and Δ of 32, although the TMR ratio showed a low value of 23%.[32]

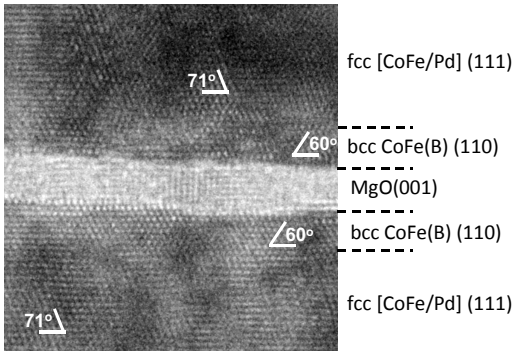

Fig. 3. Cross-sectional high resolution transmission electron microscopy (HRTEM) image for a $[Co_{90}Fe_{10}(0.2)/Pd(1.2)]$ multilayer/$Co_{20}Fe_{60}B_{20}(1.8)$/MgO(2.1)/$Co_{20}Fe_{60}B_{20}(1.8)$/$[Pd(1.2)/Co_{90}Fe_{10}(0.2)]$ multilayer stack annealed at 300°C.

3.3. *Multilayers*

For p-MTJs, I_{C0} and Δ are in a trade-off relation as can be seen in Eq. (1). In order to reduce I_{C0}, it is necessary to moderately reduce Δ. From this viewpoint, multilayer electrodes have advantages; it is relatively easy to control M_S and H_K for multilayer by changing the number of the layer stack and the layer thicknesses. In addition, multilayer films are comparatively easy to realize perpendicular magnetic easy axis. Several groups have presented that perpendicular easy axis can be achieved in Co/Pd, Co/Pt, Co/Au and Co/Ni multilayers.[49−52] The perpendicular magnetic anisotropy is originated from interfacial anisotropy.[53] In Co/Au multilayers, giant magnetoresistance (MR) effect has also been observed.[54,55] MR ratios of CPP-GMR pillars using Co/Ni or CoFe/Pt multilayer electrodes with perpendicular easy axis and Cu interlayer in which STT switching was observed for the first time were 1% or less.[31,56] Then, a MR ratio of 7% for CPP-GMR devices using CoFe/Pd multilayer electrodes and Cu interlayer was reported.[57] Thereafter, MTJs with multilayer were studied actively in order to obtain a high TMR ratio. TMR ratio was developed up to 15% in the AlO_x barrier p-MTJs.[58−61] High TMR was not obtained in the earlier stage of development of MgO barrier p-MTJ multilayer electrodes.[62] Subsequently, it was reported that the insertion of CoFeB between MgO barrier and CoFe/Pd multilayer electrodes results in a TMR ratio of 91% at $T_a = 250$°C, but it rapidly decreases below 5% at $T_a = 275$°C.[63,64] The bcc(110) oriented crystallization upon annealing of the initially amorphous CoFe(B) layers adjacent to MgO barrier, as shown in Fig. 3, is one of the reasons for the low TMR ratios,[63,65] because high TMR ratios require bcc (001) oriented ferromagnetic electrodes and MgO (001) barrier for the coherent tunneling of Δ_1 band electrons.[21,22] In these structures, CoFeB is adjacent to fcc(111)-Pd, which has a finite solid solubility of B (18% in bulk).[66] The diffusion of B from CoFeB into the CoFe/Pd multilayer is believed to cause the unwanted crystallization of CoFeB from the multilayer side because crystallization of CoFeB is known to be triggered by the loss of B.[62,63,65] By employing the thin Pd layer near an atomic monolayer, the TMR ratio became 113% at $T_a = 300$°C and 100% at $T_a = 350$°C.[67,68] The improvement of annealing stability in TMR properties is attributed to the increase of crystallization temperature of CoFe(B) resulting from the increase of the amount of residual B atoms in the CoFe(B) layer because of the limited amount of soluble B in thin Pd layer. It has been demonstrated that the p-MTJs with thin bottom Co/Pt superlattice by using nearly atomic-monolayer alternation of Co and Pt can show TMR ratios of 62−85% in the low resistance−area product RA range of 3.9−4.4 $\Omega\mu m^2$.[69,70] These multilayer electrode systems are expected to satisfy the requirements for reference layer. As to the use for a recording layer, studies of α[71−74] and TMR properties are needed.

3.4. *CoFeB-MgO*

In 2010, a perpendicular magnetic easy axis was reported in Ta/CoFeB/MgO stacks with a thin CoFeB, where the CoFeB−MgO interface anisotropy

plays a crucial role.[33,75–77] According to first-principles calculation, the interfacial perpendicular anisotropy between oxide and ferromagnetic metal has been attributed to hybridization of Fe 3d and O 2p orbitals.[78] Although earlier experimental studies also indicated the presence of perpendicular anisotropy at the interface in Pt−Co(FeB)−MO_x (M = Al, Mg, Ta and Ru) trilayer structures,[79–81] the origin of the anisotropy was ambiguous because these structures always contained Pt adjacent to ferromagnetic metals to stabilize the perpendicular anisotropy.

In the following, we review the properties of p-MTJs utilizing the CoFeB/MgO stack system. The MTJ structures consist of, from the substrate side, Ta(5)/Ru(10)/Ta(5)/$Co_{20}Fe_{60}B_{20}$(0.9−1.3)/MgO (0.85−1.05)/$Co_{20}Fe_{60}B_{20}$(1.5−1.7)/Ta(5)/Ru(5) (numbers in parenthesis are nominal thicknesses in nanometers), which are processed into circular devices by electron-beam lithography and Ar-ion milling. Figure 4 is a cross-sectional TEM image of a p-MTJ structure annealed at 300°C, showing flat interfaces. The top and bottom CoFeB layers are continuous and appear not to have fully crystallized. The top CoFeB/Ta interface looks more indistinct than the bottom Ta/CoFeB interface, which is consistent with the fact that the CoFeB/Ta stacks (corresponding to the top electrodes in the MTJs) have approximately 0.4−0.5 nm-thick magnetically dead layer evaluated from the product of saturation magnetic moment and CoFeB thickness (t_{CoFeB}) versus t_{CoFeB} curve (not shown) and the Ta/CoFeB/MgO stacks (corresponding to the bottom electrodes) have no signature of a dead layer.

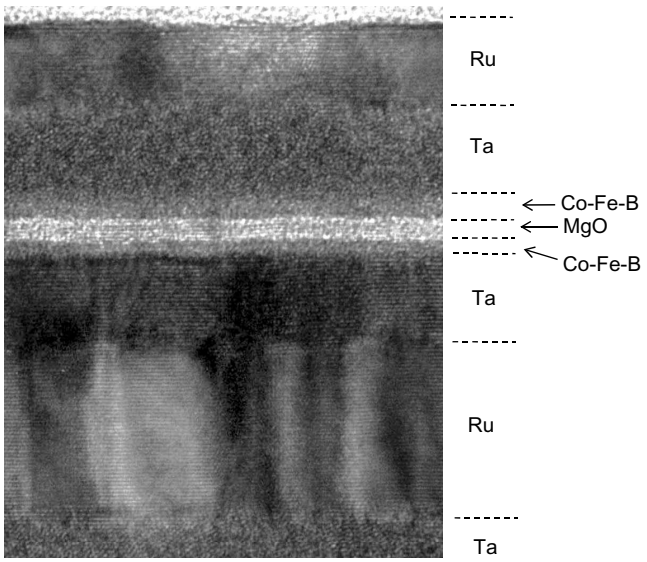

Fig. 4. Cross-sectional TEM image for a CoFeB/MgO/CoFeB p-MTJ structure annealed at 300°C.

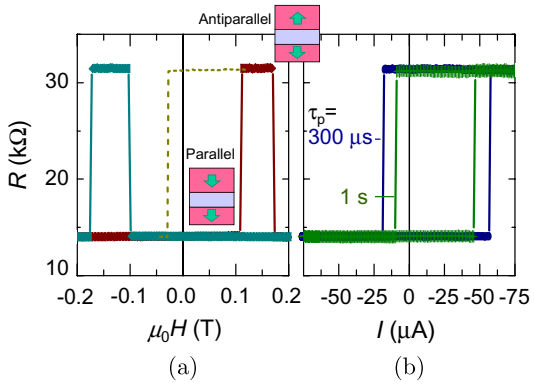

Fig. 5. (a) Out-of-plane $R-H$ curves in the CoFeB−MgO p-MTJ annealed at 300°C. The filled symbols and dashed line represent major and minor loops respectively. (b) $R-I$ curves at current-pulse durations of 300 μs and 1.0 s.

Figure 5(a) shows an out-of plane $R-H$ curve of a CoFeB−MgO based p-MTJ with 40 nm in diameter annealed at 300°C. The top and bottom CoFeB thicknesses t_{CoFeB} of the MTJ are 1.7 nm and 1.0 nm, respectively and MgO thickness t_{MgO} is 0.85 nm. The MTJ is annealed at 300°C (350°C)[82] for 1 h. The TMR ratio is 124% (113%) with resistance−area product $RA = 18\ \Omega\mu m^2$ (16 $\Omega\mu m^2$). Thus, degradations of TMR ratio and RA were not observed after annealing of 350°C. The minor loop of the recording layer (the recording layer is identified from the STT measurement as mentioned below) is shifted by 37 mT with respect to $H = 0$, indicating the existence of dipolar interlayer coupling between the two CoFeB layers. Figure 5(b) shows the resistance versus current curves ($R-I$ curves) measured at two current-pulse durations $\tau_P = 300\,\mu$s and 1.0 s, without an external magnetic field. Clear switching in the $R-I$ curves is observed. From the relationship between the current polarity and switched magnetization configuration, we can identify the top CoFeB layer to be the recording layer. From linear fits of switching current I_C versus $\ln(\tau_P/\tau_0)$, we can obtain I_{C0} at $\ln(\tau_P/\tau_0) = 0$ and Δ from its slope,[83] where τ_0 is the inverse of the attempt frequency assumed to be 1 ns. Figure 6 shows I_{C0} for p-MTJs as a function of the recording layer area (S_{rec}), where t_{CoFeB} are 0.9 nm and 1.5 nm for bottom and top CoFeB layers, respectively, t_{MgO} is 0.9 nm. The I_{C0} increases almost linearly with increasing S_{rec}, indicating that the switching current

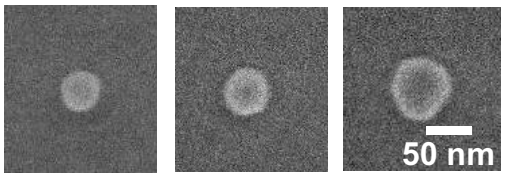

(a)

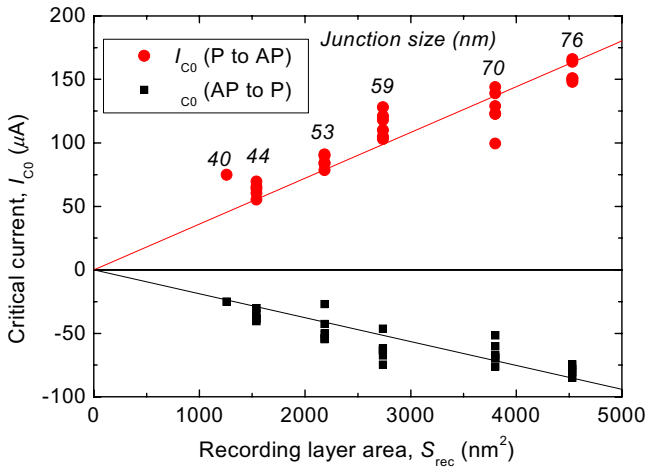

(b)

Fig. 6. (a) Top view of MTJ pillars with different junction sizes taken by SEM. (b) Critical current (I_{C0}) of CoFeB−MgO p-MTJs as a function of the recording layer area S_{rec}.

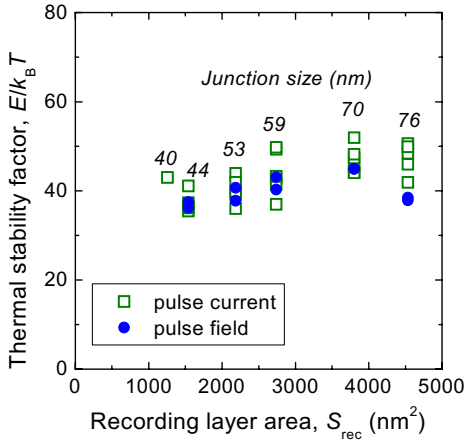

(a)

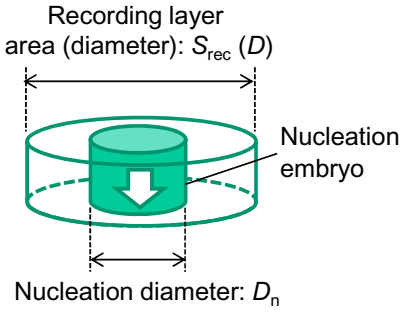

(b)

Fig. 7. (a) Thermal stability factor ($\Delta = E/k_BT$) of CoFeB−MgO p-MTJs as a function of the recording layer area S_{rec}. (b) Schematic diagram of nucleation type magnetization reversal.

is scalable. On the other hand, the Δ maintains almost constant values even though the S_{rec} is varied from ∼5000 nm^2 to ∼1500 nm^2, as can be seen in Fig. 7(a). The Δ values evaluated by pulse current experiments agree well with the results obtained from switching probability measurement by pulse magnetic field.[84] The relationship between Δ and S_{rec} indicates that only a portion of S_{rec} contributes to the thermal stability of the recording layer. This behavior can be explained by nucleation type magnetization reversal,[85,86] as found in perpendicular-patterned media.[87–91] Figure 7(b) shows a schematic of the nucleation type magnetization reversal. The diameter of nucleation size D_n is found to be approximately 40 nm and almost independent of junction size.[85] The D_n value is close to the domain wall width d_w ($\sim \pi(A_S/K_{eff})^{1/2}$) as found in media studies by using A_S determined by a separate study,[92] where A_S is the exchange stiffness constant and K_{eff} is effective magnetic anisotropy energy density. The values of Δ in the junction size range of 40−80 nm in diameter also increase linearly as the CoFeB recording layer thickness increases.[93]

Table 1 summarizes characteristics of reported p-MTJs. The first and second rows of Table 1 are typical properties of i-MTJs.[94,95] Meanwhile, the results of CoFeB-MgO p-MTJ system are shown below the 20th row in Table 1. Typical properties for our results on CoFeB-MgOp-MTJs with 40 nmϕ annealed at $T_a = 300$°C and 350°C are shown in the 20th and 21st rows of Table 1 at Refs. 33 and 82. The I_{C0}/Δs in p-MTJs are smaller than those of i-MTJs, that is, p-MTJs have a high potential for realizing low current while maintaining high Δ. In addition, the CoFeB−MgO MTJ satisfies most of the requirements at dimension as low as 40 nmϕ, except for the switching current (∼48 μA), which is slightly higher than $F(40)$ μA. Further improvements in thermal stability and annealing tolerance can be expected by suppressing dipolar interlayer coupling between the two CoFeB layers.[96,97] A fast switching speed by STT[98] and low write error rate[99]

Table 1. Comparison of MTJ characteristics.

Row	Type	Barrier/Recording layer structure (nm)	Size (nm)	TMR (%)	$RA(\Omega\mu m^2)$	J_{C0} (MA/cm^2)	$I_{C0}[I_C]$ (μA)	$\Delta = E/k_BT$	I_{C0}/Δ	T_a(°C)	Ref.
1	i-MTJ	MgO/CoFeB(2)/Ru(0.65)/ CoFeB(1.8)	100 × 200	>130	∼10	2	∼400	65	∼6.2	300	94
2	i-MTJ	MgO/CoFeB(2.4)/MgO(0.4)	100 × 200	>110	∼20	3	600	41	15	300	95
3	p-MTJ	GdFeCo(50)/CoFe/Al_2O_3	85 k × 85 k	55	6.5 M	—	—	—	—	—	34
4	p-MTJ	AlOx/GdFeCo/FeCo/AlO_x	3.5 k × 2.5 k	74	—	—	—	—	—	—	35
5	p-MTJ	GdFeCo(100)/Fe(3)/MgO	Blanket	64 (CIPTt[a])	35 k	—	—	—	—	—	36
6	p-MTJ	TbFeCo/P_6O_{11}	200 k × 200 k	70	—	—	—	—	—	—	37
7	p-MTJ	MgO/FeCo(1 -1.5)/TbFe(5)	3 k × 6 k	9.5	3 k	—	—	—	—	—	41
8	p-MTJ	MgO/CoFeB(1)/TbCoFe(3)	130 φ	∼15	—	4.7	650	107	6.08	—	38
9	p-MTJ	AlO_x/CoFe/Pt/Co/Pt	800	8	100 M	—	—	—	—	200	59
10	p-MTJ	AlO_x/[Co(0.7)/Pt(1.8)]	6.5 k × 4 k	15	—	—	—	—	—	—	58
11	p-MTJ	AlO_x/[Co(0.8)/Pt(2)]	>8 k × 4 k	14.7	30 k	—	—	—	—	170	61
12	p-MTJ	[Co/Pt]CoFeB/CoFe/MgO	Blanket	85–97 (CIPT)	4.4–10	—	—	—	—	225	69
13	p-MTJ	MgO/CoFeB/[CoFe/Pd]	>800 × 800	100 (113)	18.7 k (20.2 k)	—	—	—	—	350 (325)	68
14	p-MTJ	[Co/Pt]/CoFeB/MgO	Blanket	62 (CIPT)	3.9	—	—	—	—	250	70
15	p-MTJ	Mg(0.4)/MgO(1.5)/$L1_0$-FePt(t)	Blanket	120 (CIPT)	11.8 k	—	—	—	—	500	46
16	p-MTJ	$L1_0$-FePt/CoFeB/MgO(1.5)/ CoFeB/Co superlattice	Blanket	202 (CIPT)	—	—	—	—	—	—	48
17	p-MTJ	$L1_0$-alloy	50–55 φ	—	—	—	49	56	0.88	—	5
18	p-MTJ	Fe based (1.5)	50 φ	22	—	2.3	46	45	1.0	—	32
19	p-MTJ	Fe based (1.5)	50 φ	23	18	1.0	20 [9]	32	0.63	—	32
20	p-MTJ	MgO/CoFeB(∼1.7)/Ta	40 φ	124	18	3.9	49	43	1.14	300	33
21	p-MTJ	MgO/CoFeB(∼1.7)/Ta	40 φ	113	16	3.8	48	39	1.23	350	82
22	p-MTJ	Ta/CoFeB/MgO	110 φ	47	13	2.0	193	45	4.3	240	98
23	p-MTJ	MgO/CoFeB/Ta	17 × 40	70	8	—	44	34	1.3	—	114
24	p-MTJ	Ta/CoFeB/MgO	∼20 φ	56	∼18	—	29	29.4	0.99	240	115
25	p-MTJ	MgO/ferromagnetic-alloy/ MgO	∼20 φ	—	—	—	—	66	∼2	—	101
26	p-MTJ	MgO/CoFeB/Ta/CoFeB/ MgO	70 φ	84	20	3.2	123	95	1.3	300	100

[a]CIPT: current-in-plane tunneling method.

have also been demonstrated. Other rows in Table 1 show p-MTJs with rare-earth/transition metal alloy, $L1_0$-ordered (Co, Fe)−Pt alloy or multilayer electrodes. Recently, it has been shown that double-interface MgO/CoFeB (1.6)/Ta (0.4)/CoFeB (1.0)/MgO recording structure increases Δ up to 95 in a larger junction size range than nucleation size, while keeping comparable intrinsic critical current with comparison to single interface CoFeB−MgO recording structure,[100] which can be understood by a decrease of α upon increasing total CoFeB recoding layer thickness.[33] Similar behavior with 20 nmϕ was recently presented by other group.[101] It has been reported that Co_2FeAl full-Heusler alloy film in direct contact with MgO also shows perpendicular easy axis[102]; TMR ratios of 53%−91% were observed in p-MTJs using a bottom Co_2FeAl electrode and a top CoFeB electrode with and without Fe(Co) insertion.[103] In addition, electric-field control of magnetism such as the change of coercivity and the magnetization reversal has been experimentally shown on CoFeB−MgO p-MTJs.[104−106]

3.5. *Other alloy materials*

In order to scale the switching current, a low α is required while maintaining a high thermal stability. $L1_0$-Mn-based alloys (i.e., MnGa[107−111] and MnAl[112]) which satisfy both of high thermal stability and low α are candidates for realizing such a recording layer. In p-MTJs with $Mn_{62}Ga_{38}$/MgO/CoFeB stack, TMR ratio of 5% at RT was observed. Insertion of Co between GaMn and MgO contributes to enhance TMR ratio up to 32%.[113]

4. Summary

The p-MTJs consisting of rare-earth/transition metal alloy, $L1_0$-ordered (Co, Fe)−Pt alloy or multilayer electrodes have not realized low I_{C0} and high Δ at the same time. On the other hand, the 40 nmϕ p-MTJs with single CoFeB−MgO interface have a high potential with a STT switching with low I_{C0} and a high Δ in meeting major requirements for integrating MTJs with CMOS. In addition, by employing double-interface MgO/CoFeB/ultrathin-Ta/CoFeB/MgO recording structure, Δ enhances while keeping I_{C0} in comparison with single-interface CoFeB−MgO recording structure. The ferromagnetic-alloy/oxide interfacial anisotropy technology in addition to low α material is an indispensable building block for realization of high performance p-MTJ in reduced dimensions.

Acknowledgments

This work was supported by the "Funding Program for World-Leading Innovative R&D on Science and Technology (FIRST Program)" of the Japan Society for the Promotion of Science (JSPS). The authors would like to thank I. Morita, T. Hirata, H. Iwanuma, N. Ohshima, M. Murahata and C. Igarashi for their technical support.

References

1. H. Ohno, T. Endoh, T. Hanyu, N. Kasai and S. Ikeda, *IEDM Tech. Dig.* (2010), p. 218.
2. S. Ikeda, J. Hayakawa, Y. M. Lee, F. Matsukura, Y. Ohno, T. Hanyu and H. Ohno, *IEEE Trans. Electron Devices* **54**, 991 (2007).
3. M. Hosomi, H. Yamagishi, T. Yamamoto, K. Bessho, Y. Higo, K. Yamane, H. Yamada, M. Shoji, H. Hachino, C. Fukumoto, H. Nagao and H. Kano, *IEDM Tech. Dig.* (2005), p. 459.
4. T. Kawahara, R. Takemura, K. Miura, J. Hayakawa, S. Ikeda, Y. M. Lee, R. Sasaki, Y. Goto, K. Ito, T. Meguro, F. Matsukura, H. Takahashi, H. Matsuoka and H. Ohno, *IEEE J. Solid-State Circuits* **43**, 109 (2008).
5. T. Kishi, H. Yoda, T. Kai, T. Nagase, E. Kitagawa, M. Yoshikawa, K. Nishiyama, T. Daibou, M. Nagamine, M. Amano, S. Takahashi, M. Nakayama, N. Shimomura, H. Aikawa, S. Ikegawa, S. Yuasa, K. Yakushiji, H. Kubota, A. Fukushima, M. Oogane, T. Miyazaki and K. Ando, *IEDM Tech. Dig.* (2008), p. 309.
6. R. Takemura, T. Kawahara, K. Miura, H. Yamamoto, J. Hayakawa, N. Matsuzaki, K. Ono, M. Yamanouchi, K. Ito, H. Takahashi, S. Ikeda, H. Hasegawa, H. Matsuoka and H. Ohno, *IEEE J. Solid-State Circuits* **45**, 869 (2010).
7. K. Tsuchida, T. Inaba, K. Fujita, Y. Ueda, T. Shimizu, Y. Asao, T. Kajiyama, M. Iwayama, K. Sugiura, S. Ikegawa, T. Kishi, T. Kai, M. Amano, N. Shimomura, H. Yoda and Y. Watanabe, *ISSCC Dig. Tech. Pap.* (2010), p. 258.
8. D. C. Worledge, G. Hu, P. L. Trouilloud, D. W. Abraham, S. Brown, M. C. Gaidis, J. Nowak, E. J. O'Sullivan, R. P. Robertazzi, J. Z. Sun and W. J. Gallagher, *IEDM Tech. Dig.* (2010), p. 296.
9. S. Chung, K. M. Rho, S. D. Kim, H. J. Suh, D. J. Kim, H. J. Kim, S. H. Lee, J. H. Park, H. M. Hwang, S. M. Hwang, J. Y. Lee, Y. B. An, J. U. Yi,

Y. H. Seo, D. H. Jung, M. S. Lee, S. H. Cho, J. N. Kim, G. J. Park, G. Jin, A. D. Smith, V. Nikitin, A. Ong, X. Tang, Y. Kim, J. S. Rho, S. K. Park, S. W. Chung, J. G. Jeong and S. J. Hong, *IEDM Tech. Dig.* (2010), p. 304.

10. A. Mochizuki, H. Kimura, M. Ibuki and T. Hanyu, *IEICE Trans. Fundam.* **E88-A**, 1408 (2005).
11. S. Matsunaga, J. Hayakawa, S. Ikeda, K. Miura, H. Hasegawa, T. Endoh, H. Ohno and T. Hanyu, *Appl. Phys. Express* **1**, 091301 (2008).
12. D. Suzuki, M. Natsui, S. Ikeda, H. Hasegawa, K. Miura, J. Hayakawa, T. Endoh, H. Ohno and T. Hanyu, Fabrication of a nonvolatile lookup-table circuit chip using magneto/semiconductor-hybrid structure for an immediate-power-up field programmable gate array, in *IEEE Symp. VLSI Circuits* (2009), p. 80.
13. W. Zhao, C. Chappert, V. Javerliac and J.-P. Noziere, *IEEE Trans. Magn.* **45**, 3784 (2009).
14. S. Matsunaga, A. Katsumata, M. Natsui, S. Fukami, T. Endoh, H. Ohno and T. Hanyu, Fully parallel 6T-2MTJ nonvolatile TCAM with single-transistor-based self match-line discharge control, in *IEEE Symp. VLSI Circuits* (2011), p. 298.
15. S. Matsunaga, S. Miura, H. Honjou, K. Kinoshita, S. Ikeda, T. Endoh, H. Ohno and T. Hanyu, A 3.14 um^2 4T-2MTJ-cell fully parallel TCAM based on nonvolatile logic-in-memory architecture, in *IEEE Symp. VLSI Circuits* (2012), p. 44.
16. T. Ohsawa, H. Koike, S. Miura, H. Honjo, K. Tokutome, S. Ikeda, T. Hanyu, H. Ohno and T. Endoh, 1Mb 4T-2MTJ nonvolatile STT-RAM for embedded memories using 32b fine-grained power gating technique with 1.0s/200ps wake-up/power-off times, in *IEEE Symp. VLSI Circuits* (2012), p. 46.
17. J. C. Slonczewski, *J. Magn. Magn. Mater.* **159**, L1 (1996).
18. L. Berger, *Phys. Rev. B* **54**, 9353 (1996).
19. J. A. Katine, F. J. Albert, R. A. Buhrman, E. B. Myers and D. C. Ralph, *Phys. Rev. Lett.* **84**, 3149 (2000).
20. F. J. Albert, J. A. Katine, R. A. Buhrman and D. C. Ralph, *Appl. Phys.Lett.* **77**, 3809 (2000).
21. W. H. Butler, X.-G. Zhang, T. C. Schulthess and J. M. MacLaren, *Phys. Rev. B* **63**, 054416 (2001).
22. J. Mathon and A. Umerski, *Phys. Rev. B* **63**, 220403 (2001).
23. S. Yuasa, A. Fukushima, T. Nagahama, K. Ando and Y. Suzuki, *Jpn. J. Appl. Phys.* **43**, L588 (2004).
24. S. Yuasa, T. Nagahama, A. Fukushima, Y. Suzuki and K. Ando, *Nature Mater.* **3**, 868 (2004).
25. S. S. P. Parkin, C. Kaiser, A. Panchula, P. M. Rice, B. Hughes, M. Samant and S. H. Yang, *Nature Mater.* **3**, 662 (2004).
26. D. D. Djayaprawira, K. Tsunekawa, M. Nagai, H. Maehara, S. Yamagata, N. Watanabe, S. Yuasa, Y. Suzuki and K. Ando, *Appl. Phys. Lett.* **86**, 092502 (2005).
27. J. Hayakawa, S. Ikeda, F. Matsukura, H. Takahashi and H. Ohno, *Jpn. J. Appl. Phys.* **44** L587 (2005).
28. S. Ikeda, J. Hayakawa, Y. Ashizawa, Y. M. Lee, K. Miura, H. Hasegawa, M. Tsunoda, F. Matsukura and H. Ohno, *Appl. Phys. Lett.* **93**, 082508 (2008).
29. C. J. Lin, S. H. Kang, Y. J. Wang, K. Lee, X. Zhu, W. C. Chen, X. Li, W. N. Hsu, Y. C. Kao, M. T. Liu, W. C. Chen, Y. C. Lin, M. Nowak, N. Yu and L. Tran, *IEDM Tech. Dig.* (2009), p. 279.
30. Y. Huai, Y. Zhou, Z. Wang, R. Malmhall, R. Ranjan and J. Zhang, STT MRAM: recent strong semiconductor industry traction, The 2nd CSIS International Symposium on Spintronics-based VLSIs and The 8th RIEC International Workshop on Spintronics (2012), p. 19.
31. S. Mangin, D. Ravelosona, J. A. Katine, M. J. Carey, B. D. Terris and E. E. Fullerton, *Nature Mater.* **5**, 210 (2006).
32. H. Yoda, T. Kishi, T. Nagase, M. Yoshikawa, K. Nishiyama, E. Kitagawa, T. Daibou, M. Amano, N. Shimomura, S. Takahashi, T. Kai, M. Nakayama, H. Aikawa, S. Ikegawa, M. Nagamine, J. Ozeki, S. Mizukami, M. Oogane, Y. Ando, S. Yuasa, K. Yakushiji, H. Kubota, Y. Suzuki, Y. Nakatani, T. Miyazaki and K. Ando, *Curr. Appl. Phys.* **10**, e87 (2010).
33. S. Ikeda, K. Miura, H. Yamamoto, K. Mizunuma, H. D. Gan, M. Endo, S. Kanai, J. Hayakawa, F. Matsukura and H. Ohno, *Nature Mater.* **9**, 721 (2010).
34. N. Nishimura, T. Hirai, A. Koganei, T. Ikeda, K. Okano, Y. Sekiguchi and Y. Osada, *J. Appl. Phys.* **91**, 5246 (2002).
35. A. C. Cabrera, C. H. Chang, C. C. Hsu, M. C. Weng, C. C. Chen, C. T. Chao, J. C. Wu, Y. H. Chang and T. H. Wu, *IEEE Trans. Magn.* **43**, 914 (2007).
36. H. Ohmori, T. Hatori and S, Nakagawa, *J. Appl. Phys.* **103**, 07A911 (2008).
37. N. N. Krupa, *JETP Lett.* **87**, 548 (2008).
38. M. Nakayama, T. Kai, N. Shimomura, M. Amano, E. Kitagawa, T. Nagase, M. Yoshikawa, T. Kishi, S. Ikegawa and H. Yoda, *J. Appl. Phys.* **103**, 07A710 (2008).
39. P. Hansen, C. Clausen, G. Much, M. Rosenkranz and K. Witter, *J. Appl. Phys.* **66**, 756 (1989).
40. T. J. Chen, A. Canizo-Cabrera, C. H. Chang, K. A. Liao, S. C. Li, C. K. Hou and T. H. Wu, *J. Appl. Phys.* **99**, 08T313 (2006).
41. L. X. Ye, C. M. Lee, J. M. Lee, J. H. Lin, J. Z. Liu, J. C. Wu and T. H. Wu, *IEEE Trans. Magn.* **47**, 3857 (2011).

42. T. Klemmer, D. Hoydick, H. Okumura, B. Zhang and W. A. Soffa, *Scr. Metall. Mater.* **33**, 1793 (1995).
43. D. Weller, A. Moser, L. Folks, M. E. Best, W. Lee, M. F. Toney, M. Schwickert, J. U. Thiele and M. F. Doerner, *IEEE. Trans. Magn.* **36**, 10 (2000).
44. T. Seki, S. Mitani, K. Yakushiji and K. Takanashi, *Appl. Phys. Lett.* **88**, 172504 (2006).
45. G. Kim, Y. Sakuraba, M. Oogane, Y. Ando and T. Miyazaki, *Appl. Phys. Lett.* **92**, 172502 (2008).
46. M. Yoshikawa, E. Kitagawa, T. Nagase, T. Daibou, M. Nagamine, K. Nishiyama, T. Kishi and H. Yoda, *IEEE Trans. Magn.* **44**, 2573 (2008).
47. Y. Taniguchi, Y. Miura, K. Abe and M. Shirai, *IEEE Trans. Magn.* **44**, 2585 (2008).
48. H. Yoda, *Magnetics Jpn.* **5**, 184 (2010) [in Japanese].
49. H. J. G. Draaisma, F. J. A. den Broeder and W. J. M. de Jonge, *J. Appl. Phys.* **63**, 3479 (1988).
50. P. F. Carcia, *J. Appl. Phys.* **63**, 5066 (1988).
51. G. Gubbiotti, G. Carlotti, F. Albertini, F. Casoli, E. Bontempi, L. E. Depero, P. Mengucci, A. Di Cristoforo, H. Koo and R. D. Gomez, *J. Appl. Phys.* **93**, 7241 (2003).
52. G. H. O. Daalderop, P. J. Kelly and F. J. A. den Broeder, *Phys. Rev. Lett.* **68**, 682 (1992).
53. M. T. Johnson, P. J. H. Bloemen, F. J. A. den Broeder and J. J. de Vries, *Rep. Prog. Phys.* **59**, 1409 (1996).
54. C. Dupas, J. P. Renard, J. Seiden, E. Vélu and D. Renard, *J. Appl. Phys.* **63**, 4300 (1988).
55. T. Takahara, S. Araki and T. Shinjo, *J. Magn. Magn. Mater.* **82**, 287 (1989).
56. H. Meng and J. P. Wang, *Appl. Phys. Lett.* **88**, 172506 (2006).
57. R. Law, R. Sbiaa, T. Liew and T. C. Chong, *Appl. Phys. Lett.* **91**, 242504 (2007).
58. J. H. Park, C. Park, T. Jeong, M. T. Moneck, N. T. Nufer and J. G. Zhu, *J. Appl. Phys.* **103**, 07A917 (2008).
59. C. Ducruet, B. Carvello, B. Rodmacq, S. Auffret, G. Gaudin and B. Dieny, *J. Appl. Phys.* **103**, 07A918 (2008).
60. B. Carvello, C. Ducruet, B. Rodmacq, S. Auffret, E. Gautier, G. Gaudin and B. Dieny, *Appl. Phys. Lett.* **92**, 102508 (2008).
61. Y. Wang, W. X. Wang, H. X. Wei, B. S. Zhang, W. S. Zhan and X. F. Han, *J. Appl. Phys.* **107**, 09C711 (2010).
62. J. H. Park, S. Ikeda, H. Yamamoto, H. D. Gan, K. Mizunuma, K. Miura, H. Hasegawa, J. Hayakawa, K. Ito, F. Matsukura and H. Ohno, *IEEE Trans. Magn.* **45**, 3476 (2009).
63. K. Mizunuma, S. Ikeda, J. H. Park, H. Yamamoto, H. D. Gan, K. Miura, H. Hasegawa, J. Hayakawa, F. Matsukura and H. Ohno, *Appl. Phys. Lett.* **95**, 232516 (2009).
64. K. Mizunuma, S. Ikeda, H. Yamamoto, H. D. Gan, K. Miura, H. Hasegawa, J. Hayakawa, K. Ito, F. Matsukura and H. Ohno, *Jpn. J. Appl. Phys.* **49**, 04DM04 (2009).
65. S. V. Karthik, Y. K. Takahashi, T. Ohkubo, K. Hono, H. D. Gan, S. Ikeda and H. Ohno, *J. Appl. Phys.* **111**, 083922 (2012).
66. T. B. Massalski, H. Okamoto, P. R. Subramanian and L. Kacprak: in *Binary Alloy Diagrams*, 2nd edn. (ASM International, Materials Park, OH, USA, (1990).
67. K. Mizunuma, M. Yamanouchi, S. Ikeda, H. Yamamoto, H. D. Gan, K. Miura, J. Hayakawa, F. Matsukura and H. Ohno, *Appl. Phys. Express* **4**, 023002 (2011).
68. K. Mizunuma, S. Ikeda, H. Sato, M. Yamanouchi, H. D. Gan, K. Miura, H. Yamamoto, J. Hayakawa, F. Matsukura and H. Ohno, *J. Appl. Phys.* **109**, 07C711 (2011).
69. K. Yakushiji, K. Noma, T. Saruya, H. Kubota, A. Fukushima, T. Nagahama, S. Yuasa and K. Ando, *Appl. Phys. Express* **3**, 053003 (2010).
70. K. Yakushiji, T. Saruya, H. Kubota, A. Fukushima, T. Nagahama, S. Yuasa and K. Ando, *Appl. Phys. Lett.* **97**, 232508 (2010).
71. A. Barman, S. Wang, O. Hellwig, A. Berger and E. E. Fullerton and H. Schmidt, *J. Appl. Phys.* **101**, 09D102 (2007).
72. E. P. Sajitha, J. Walowski, D. Watanabe, S. Mizukami, F. Wu, H. Naganuma, M. Oogane, Y. Ando and T. Miyazaki, *IEEE Trans. Magn.* **46**, 2056 (2010).
73. S. Mizukami, E. P. Sajitha, D. Watanabe, F. Wu, T. Miyazaki, H. Naganuma, M. Oogane and Y. Ando, *Appl. Phys. Lett.* **96**, 152502 (2010).
74. S. Mizukami, X. Zhang, T. Kubota, H. Naganuma, M. Oogane, Y. Ando and T. Miyazaki, *Appl. Phys. Express* **4**, 013005 (2011).
75. M. Endo, S. Kanai, S. Ikeda, F. Matsukura and H. Ohno, *Appl. Phys. Lett.* **96**, 212503 (2010).
76. S. Kanai, M. Endo, S. Ikeda, F. Matsukura and H. Ohno, *J. Phys.: Conf. Ser.* **266**, 012092 (2011).
77. M. Yamanouchi, R. Koizumi, S. Ikeda, H. Sato, K. Mizunuma, K. Miura, H. D. Gan, F. Matsukura and H. Ohno, *J. Appl. Phys.* **109**, 07C712 (2011).
78. R. Shimabukuro, K. Nakamura, T. Akiyama and T. Ito, *Physica E* **42**, 1014 (2010).
79. S. Monso, B. Rodmacq, S. Auffret, G. Casali, F. Fettar, B. Gilles, B. Dieney and P. Boyer, *Appl. Phys. Lett.* **80**, 4157 (2002).
80. A. Manchon, C. Ducruet, L. Lombard, S. Auffret, B. Rodmacq, B. Dieny, S. Pizzini, J. Vogel, V. Uhlir, M. Hochstrasser and G. Panaccione, *J. Appl. Phys.* **104**, 043914 (2008).

81. L. E. Nistor, B. Rodmancq, S. Auffretand B. Dieny, *Appl. Phys. Lett.* **94**, 012512 (2009).
82. K. Miura, S. Ikeda, M. Yamanouchi, H. Yamamoto, K. Mizunuma, H. D. Gan, J. Hayakawa, R. Koizumi, M. Endo, S. Kanai, F. Matsukura and H. Ohno, High tunnel magnetoresistance, low current switching and high thermal stability in 40-nm-diameter CoFeB/MgO-based magnetic tunnel junctions with perpendicular anisotropy, in *55th Annual Conf. on Magn. and Magn. Mater.* (2010), HC-02.
83. R. H. Koch, J. A. Katine and J. Z. Sun, *Phys. Rev. Lett.* **92**, 088302 (2004).
84. Z. Li and S. Zhang, *Phys. Rev. B* **69**, 134416 (2004).
85. H. Sato, M. Yamanouchi, K. Miura, S. Ikeda, H. D. Gan, K. Mizunuma, R. Koizumi, F. Matsukura and H. Ohno, *Appl. Phys. Lett.* **99**, 042501 (2011).
86. J. Z. Sun, R. P. Robertazzi, J. Nowak, P. L. Trouilloud, G. Hu, D. W. Abraham, M. C. Gaidis, S. L. Brown, E. J. O'Sullivan, W. J. Gallagher and D. C. Worledge, *Phys. Rev. B* **84**, 064413 (2011).
87. N. Kikuchi, K. Mitsuzuka, T. Shimatsu, O. Kitakami and H. Aoi, *J. Phys. D* **200**, 102003 (2010).
88. T. Thomson, G. Hu and B. D. Terris, *Phys. Rev. Lett.* **96**, 257204 (2006).
89. T. Aoyama, K. Uchiyama, K. Hattori, Y. Wada, S. Okawa, H. Hatate, H. Nishio and I. Sato, *IEEE. Trans. Magn.* **37**, 1646 (2001).
90. J. Moritz, B. Dieny, J. P. Nozieres, R. J. M. van. de Veerdonk, T. M. Crawford, D. Weller and S. Landis, *Appl. Phys. Lett.* **86**, 063512 (2005).
91. K. Mitsuzuka, N. Kikuchi, T. Shimatsu, O. Kitakami, H. Aoi, H. Muraoka and J. C. Lodder, *IEEE. Trans. Magn.* **43**, 2160 (2007).
92. M. Yamanouchi, A. Jander, P. Dhagat, S. Ikeda, F. Matsukura and H. Ohno, *IEEE Magn. Lett.* **2**, 3000304 (2011).
93. H. Sato, M. Yamanouchi, K. Miura, S. Ikeda, R. Koizumi, F. Matsukura and H. Ohno, *IEEE Magn. Lett.* **3**, 3000204 (2012).
94. J. Hayakawa, S. Ikeda, K. Miura, M. Yamanouchi, Y. M. Lee, R. Sasaki, M. Ichimura, K. Ito, T. Kawahara, R. Takemura, T. Meguro, F. Matsukura, H. Takahashi, H. Matsuoka and H Ohno, *IEEE Trans. Magn.* **44**, 1962 (2008).
95. H. Yamamoto, J. Hayakawa, K. Miura, K. Ito, H. Matsuoka, S. Ikeda and H. Ohno, *Appl. Phys. Express* **5**, 053002 (2012).
96. H. D. Gan, H. Sato, M. Yamanouchi, S. Ikeda, K. Miura, R. Koizumi, F. Matsukura and H. Ohno, *Appl. Phys. Lett.* **99**, 252507 (2011).
97. K. Miura, S. Ikeda, M. Yamanouchi, H. Yamamoto, K. Mizunuma, H. D. Gan, J. Hayakawa, R. Koizumi, F. Matsukura and H. Ohno, CoFeB/MgO based perpendicular magnetic tunnel junctions with stepped structure for symmetrizing different retention times of '0' and '1' information, in *IEEE Symp. VLSI Tech.* (2011), p. 214.
98. D. C. Worledge, G. Hu, D. W. Abraham, J. Z. Sun, P. L. Trouilloud, J. Nowak, S. Brown, M. C. Gaidis, J. O'Sullivan and R. P. Robertazzi, *Appl. Phys. Lett.* **98**, 022501 (2011).
99. J. J. Nowak, R. P. Robertazzi, J. Z. Sun, G. Hu, D. W. Abraham, P. L. Trouilloud, S. Brown, M. C. Gaidis, E. J. O'Sullizan, W. J. Gallagher and D. C. Worledge, *IEEE Magn. Lett.* **2**, 3000204 (2011).
100. H. Sato, M. Yamanouchi, S. Ikeda, S. Fukami, F. Matsukura and H. Ohno, *Appl. Phys. Lett.* **101**, 022414 (2012).
101. J. H. Park, Y. Kim, W. Lim, J. Kim, S. Park, J. Kim, W. Kim, K. Kim, J. Jeong, K. S. Kim, H. Kim, Y. J. Lee, S. Oh, J. E. Lee, S. O. Park, S. Watts, D. Apalkov, V. Nikitin, M. Krounbi, S. Jeong, S. Choi, H. Kang and C. Chung, in *IEEE Symp. VLSI Tech.*(2012), p. 57.
102. Z. Wen, H. Sukegawa, S. Mitani and K. Inomata, *Appl. Phys. Lett.* **98**, 242507 (2011).
103. Z. Wen, H. Sukegawa, S. Kasai, M. Hayashi, S. Mitani and K. Inomata, *Appl. Phys. Express* **5**, 063003 (2012).
104. W. G. Wang, M. Li, S. Hageman and C. L. Chien, *Nature Mater.* **11**, 64 (2012).
105. H. Meng, R. Sbiaa, M. A. K. Akhtar, R. S. Liu, V. B. Naik and C. C. Wang, *Appl. Phys. Lett.* **100**, 122405 (2012).
106. S. Kanai, M. Yamanouchi, S. Ikeda, Y. Nakatani, F. Matsukuraand H. Ohno, *Appl. Phys. Lett.* **101**, 122403 (2012).
107. B. Balke, G. H. Fecher, J. Winterlik and C. Felser, *Appl. Phys. Lett.* **90**, 152504 (2007).
108. F. Wu, S. Mizukami, D. Watanabe, H. Naganuma, M. Oogane, Y. Ando and T. Miyazaki, *Appl. Phys. Lett.* **94**, 122503 (2009).
109. S. Mizukami, F. Wu, A. Sakuma, J. Walowski, D. Watanabe, T. Kubota, X. Zhang, H. Naganuma, M. Oogane, Y. Ando and T. Miyazaki, *Phys. Rev. Lett.* **106**, 117201 (2011).
110. H. Kurt, K. Rode, M. Venkatesan, P. Stamenov and J. M. D. Coey, *Phys. Rev. B* **83** 020405(R) (2011).
111. S. Mizukami, T. Kubota, F. Wu, X. Zhang, H. Naganuma, M. Oogane, Y. Ando, A. Sakuma and T. Miyazaki, *Phys. Rev. B* **85**, 014416 (2012).
112. M. Hosoda, M. Oogane, M. Kubota, T. Kubota, H. Saruyama, S. Iihama, H. Naganuma and Y. Ando, *J. Appl. Phys.* **111**, 07A324 (2012).
113. Q. L. Ma, T. Kubota, S. Mizukami, X. M. Zhang, H. Naganuma, M. Oogane, Y. Ando and T. Miyazaki, *Appl. Phys. Lett.* **101**, 032402 (2012).

114. M. Gajek, J. J. Nowak, P. L. Trouilloud, E. J. O'Sullivan, D. W. Abraham, M. C. Gaidis, G. Hu, S. Brown, Y. Zhu, R. P. Robertazzi, W. J. Gallagher and D. C. Worledge, *Appl. Phys. Lett.* **100**, 132408 (2012).
115. Y. Kim, S. C. Oh, W. C. Lim, J. H. Kim, W. J. Kim, J. H. Jeong, H. J. Shin, K. W. Kim, K. S. Kim, J. H. Park, S. H. Park, H. Kwon, K. H. Ah, J. E. Lee, S. O. Park, S. Choi, H. K. Kang and C. Chung, Integration of 28 nm MUT for 8∼16Gb level MRAM with full investigation of thermal stability in *IEEE Symp. VLSI Tech.* (2011), p. 210.